Measurement of a Dispersion Curve for Linear-Regime Rayleigh-Taylor Growth Rates in Laser-Driven Planar Targets

S. G. Glendinning,[1] S. N. Dixit,[1] B. A. Hammel,[1] D. H. Kalantar,[1] M. H. Key,[2,3] J. D. Kilkenny,[1] J. P. Knauer,[4] D. M. Pennington,[1] B. A. Remington,[1] R. J. Wallace,[1] and S. V. Weber[1]

[1]*Lawrence Livermore National Laboratory, University of California, Livermore, California 94550*

[2]*Rutherford Appleton Laboratory, United Kingdom*

[3]*University of Oxford, United Kingdom*

[4]*Laboratory for Laser Energetics, 250 E. River Rd., Rochester, New York 14623–1299*

(Received 3 September 1996)

A dispersion curve for Rayleigh-Taylor growth rates in the linear regime has been measured in planar CH_2 laser-driven foils. The foils were ablatively accelerated with a single, smoothed, frequency-doubled beam of the Nova laser at 7×10^{13} W/cm^2 (giving an acceleration of 60 μm/ns^2). Measured growth rates were about 50% of the classical values. Growth rates simulated with the computer code LASNEX were ~18% higher than measured values. [S0031-9007(97)03035-4]

PACS numbers: 52.35.Py, 52.65.Ff, 52.70.–m

Understanding and controlling the Rayleigh-Taylor (RT) instability has long been recognized as a critical issue for the success of inertially confined fusion [1–3], particularly for implosions in which the capsule is driven directly with laser light. Capsules are now being designed [4–6] in which ignition and gain are predicted using lasers of about 2 MJ such as the National Ignition Facility. One of the keys to evaluating such a design is the ability to accurately predict RT growth at the ablation surface, where modulations are predicted in a linear analysis to grow by factors of one to several thousand. Since RT growth in the linear regime is exponential, errors in the predicted growth rates of 20% will result in errors in growth of 1–2 e-foldings. An experimental investigation of the ability to model RT growth at an ablating interface over a significant range of wavelengths is essential to the correct design of ignition capsules. Several such measurements have been made [7–10], but all used large initial amplitudes and rapidly entered the nonlinear regime where the amplitude is greater than 10% of the wavelength. In this regime the growth rate decreases from exponential to secular (saturates). Our goal in these experiments was to use small initial amplitudes to observe sufficient growth in the linear regime to determine growth rates for quantitative comparison with modeling.

In our experiment we used one beam of the Nova laser at 0.53 μm wavelength to accelerate 20 μm thick CH_2 foils (initial density 0.95g/cm^3) as shown in Fig. 1. The plastic foils each had a single mode sinusoidal modulation molded on the driven side, with wavelengths of 20, 30, 50, or 70 μm, and initial amplitudes between 0.1 and 1.0 μm. We chose initial amplitudes at each wavelength to minimize the uncertainty in the growth rate determination (mostly due to instrument noise limiting the minimum measurable amplitude). The drive laser was smoothed with a random phase plate (RPP) [11] and spectral dispersion [12] (SSD), with about 0.9 THz bandwidth. A diffraction grating gave 0.086 μrad/THz dispersion and a temporal skew of 110 ps to the pulse front. The beam was split into nine segments, each independently steered in space with a glass wedge to form a flat-topped spatial intensity distribution ($\pm 8\%$ over 700 μm). The drive pulse was a linear 1 ns ramp to an intensity of 7×10^{13} W/cm^2, followed by constant intensity at this level for 2 ns. A typical measured drive pulse is shown in Fig. 2. The shock reached the back surface of the 20 μm thick foil at about 0.7 ns after the start of the laser pulse. The foil then accelerated at about 60 μm/ns^2, allowing for 2 ns of constant acceleration to study Rayleigh-Taylor (RT) growth. During the acceleration the foil is predicted to decompress somewhat. We simulated these experiments with the two-dimensional radiation hydrodynamics code LASNEX [13]. The simulated peak density vs time is also shown in Fig. 2. In Ref. [7] we determined that our LASNEX simulations correctly predicted the acceleration and shock transit time of a foil driven with this laser configuration.

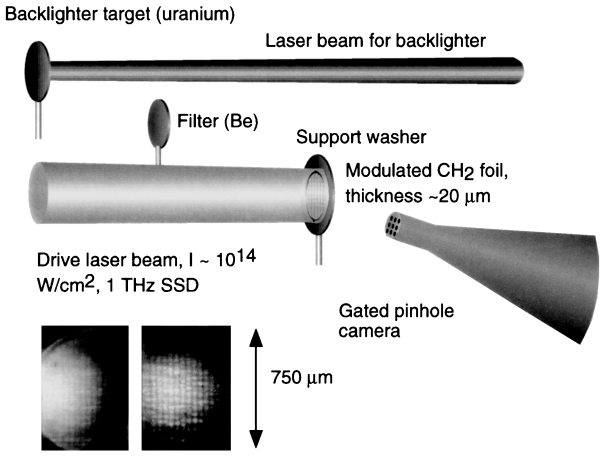

FIG. 1. Experimental setup with typical radiographs at $t =$ 1.2 ns (left) and 2.1 ns (right). Initial surface modulations with $\lambda_x = 30$ μm are visible. Imprint of the smoothed laser beam is also visible as horizontal streaks.

 0031-9007/97/78(17)/3318(4)$10.00

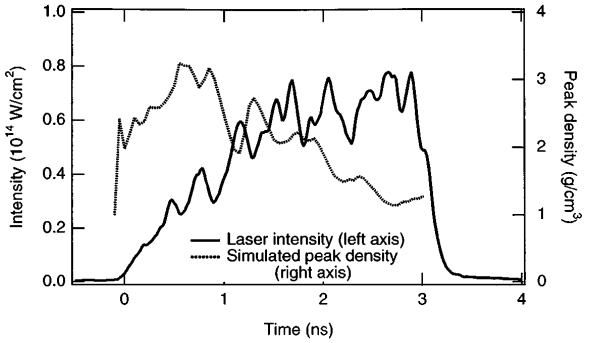

FIG. 2. Typical measured laser power history and simulated foil peak density vs time. Amplitude modulations in the laser pulse are a consequence of the bandwidth on the pulse.

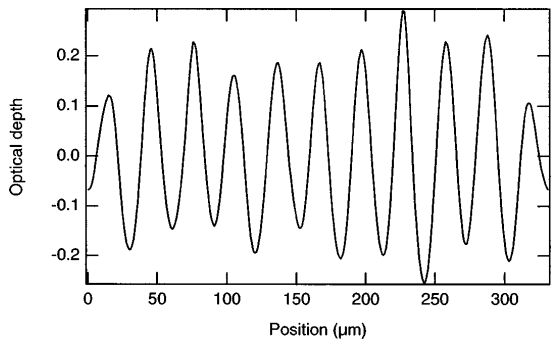

FIG. 3. Vertical profile of the image at $t = 2.1$ ns in Fig. 1 (after processing).

We measured the areal density modulations on the foils by conventional x-ray backlighting using a gated pinhole camera with 8 μm spatial and 100 ps temporal resolution [14], providing up to 12 frames per shot with arbitrary time spacing. The x-ray backlighter [15] was a uranium disk illuminated by a second 0.53 μm wavelength Nova beam (smoothed with a RPP) at about 6×10^{14} W/cm^2, giving a broad spectrum peaked at $\sim$1 keV. The foil was shielded from the backlighter with 12.7 μm Be to eliminate any effect of the low energy backlighter x-rays. Typical radiographs for a foil with modulation wavelength $\lambda = 30$ μm and initial amplitude $\eta_0 = 0.25$ μm at $t = 1.2$ and 2.1 ns are shown in Fig. 1.

Each image was analyzed by converting film density to exposure, extracting a square region, dividing by a second degree polynomial fit to remove the spatial nonuniformity of the backlighter, and filtering out high frequency noise (spatial wavelength less than 10 μm) with a Wiener filter [16]. The negative of the natural logarithm of the result is optical depth (τ), with an arbitrary zero. By averaging the resulting image across the direction of the imposed perturbation, a profile such as the one shown in Fig. 3 was constructed for each image. (This profile is for the image shown in Fig. 1 at $t = 2.1$ ns.)

Each wavelength in the profile in Fig. 3 may be decomposed into its Fourier amplitudes, giving a mean and standard error for that profile. Different frames give a set of amplitudes of the fundamental vs time on each shot. Different shots (not shown) gave the various wavelengths. For steady-state RT growth in the linear regime, the amplitudes should grow exponentially with time. The amplitudes for each shot are shown in Fig. 4(a)–4(d), as well as exponential fits. The fits were constrained to begin after $t = 1.0$ ns to avoid measuring growth during the shock transit phase.

It may be observed in Fig. 1 that the residual modulations in the drive laser result in imprinted modulations in the foil (across the direction of the imposed perturbation). In order to determine that the preimposed mode is still in the linear regime, it is essential to consider the effect of the spectrum in the neighborhood of the mode, including both imprint and the preimposed mode. Multimode effects could lead to saturation of the surface mode at a lower amplitude than expected [17]. We estimate the onset of nonlinear multimode saturation, according to the Haan model [18], by comparing η_{char}, the quadrature sum of the amplitudes within $\pm 0.4k$ ($k = 2\pi/\lambda$) of the surface mode, with 10% λ. The amplitudes are converted from optical depth to spatial amplitudes by assuming cold opacity (one optical depth at solid density corresponds to 20 μm of material), and assuming that the density is the peak compressed density at the frame time. The imprinted spectrum does not appear to significantly accelerate the onset of nonlinearity in any of our data, since η_{char} is less than 10% λ in all cases.

The growth rates obtained from the exponential fits to the data at each wavelength were averaged, and the resulting growth rates are plotted vs wavelength in Fig. 5. The error bars represent the standard deviation of the mean of the data set for the cases with multiple measurements. For the 20 μm data with only one measurement the error bar is the uncertainty in the fit. Each shot was simulated separately, using the measured drive histories, and the resulting predictions were post-processed by numerically transmitting the backlighter spectrum through the simulated foil. The resulting predicted ideal radiograph was convolved with the measured instrument response function (including the Wiener filter), and the negative of the natural logarithm of this result was Fourier decomposed. Growth rates from exponential fits to the LASNEX simulations of each shot (fit over the same time intervals as the data) are shown in Fig. 5. The error bars on the LASNEX growth rates represent the uncertainty in the exponential fits.

The measured modulation of optical depth is sensitive only to lateral material flow [19]. For our experiment, the growth rate in optical depth (γ_τ) is related to the growth rate in spatial amplitude γ_z by

$$\gamma_\tau = \gamma_z + \frac{1}{\Delta t} \ln(1 + \dot{\rho}\,\Delta t/\rho_{t=1}) \approx \gamma_z + \dot{\rho}/\rho_{t=1} \quad (1)$$

where Δt is the measurement interval, $\rho_{t=1}$ is the maximum compressed density (at $t = 1$ ns, where the fits start), and $\dot{\rho}$ is the decompression rate during Δt. LASNEX simulations predict $\dot{\rho}$ to be about -0.9 (g/cm^3)/ns and

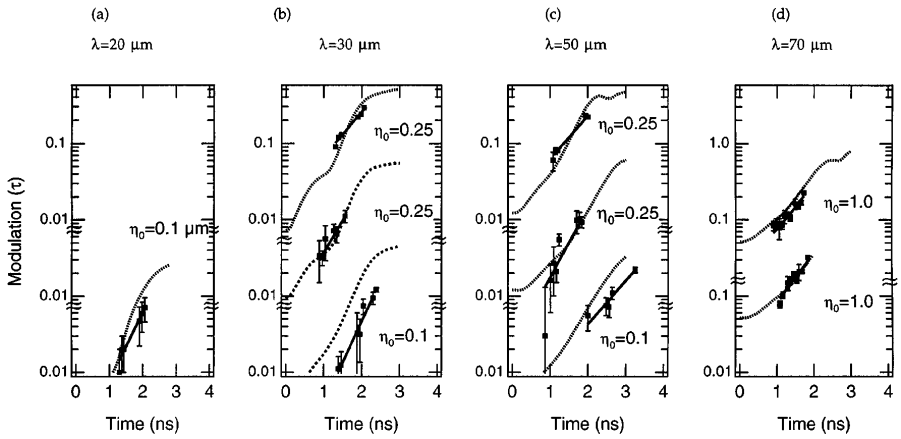

FIG. 4. Fundamental amplitude in optical depth vs time for shots at four wavelengths (solid squares), simulated amplitude in optical depth vs time for these shots (dashed lines), and exponential fits to the data (solid lines). The curves are labeled with the initial amplitude in microns. Note the vertical offsets in each plot.

$\rho_{t=1}$ about 2.5 g/cm^3. Thus the growth rates determined from optical depth are predicted to be typically about 20% smaller than the growth rates would be if determined from spatial amplitudes at the unstable interface (i.e., at the ablation surface). We observed growth rates (γ_τ) which were about 50% classical (nearly constant with wavelength); the LASNEX predictions for growth rates in optical depth decreased with wavelength, averaging about 60% classical. However, the growth rates in spatial modulation are predicted by LASNEX to be about 60%–80% classical (over 20–70 μm), as shown in Fig. 6. The reduction in γ_z from classical is due to two dominant factors, the removal of modulated material by ablation [20,21], and the finite width of the interface region, expressed by Takabe *et al.* as

$$\gamma = \alpha\sqrt{kg} - \beta k V_a\,, \tag{2}$$

where γ is the growth rate, g is the interface acceleration, k is 2π/wavelength, V_a is the ablation velocity (i.e., the rate in μm/ns at which material is removed), and α and β are adjustable parameters. A plot with $\alpha = 0.9$ and $\beta = 3.6$, obtained as the best fit in β to the LASNEX growth rates holding α at 0.9, is shown in Fig. 6 as the dashed line. A modified version of this as derived by Lindl [22] includes the finite width of the interface region explicitly rather than rather than as an arbitrary Atwood number, as

$$\gamma = \sqrt{\frac{kg}{1 + kL}} - \beta k v_a\,, \tag{3}$$

where $L = [\rho/(d\rho/dz)]_{\min}$ is the density gradient scale length. LASNEX simulations for our experiments predict L to be about 1 μm and V_a to be about 1 μm/ns. The result with $\beta = 2.0$ is also shown in Fig. 6. The prediction of Betti *et al.* [23], also shown in Fig. 6, may be expressed for this experiment as

$$\gamma = 0.90\sqrt{kg} - 3.2 k v_a\,. \tag{4}$$

In this case, the coefficients are predicted by the theory. For these conditions all the predictions appear to give indistinguishable results except at the shortest wavelengths. Our data do not extend to such short wavelengths.

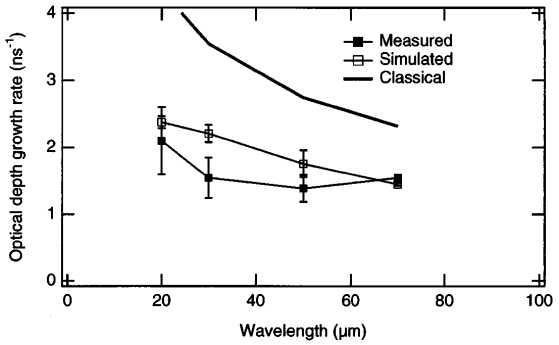

FIG. 5. Average growth rates in optical depth (γ_τ) vs wavelength. The data are solid squares and the LASNEX predictions are open squares.

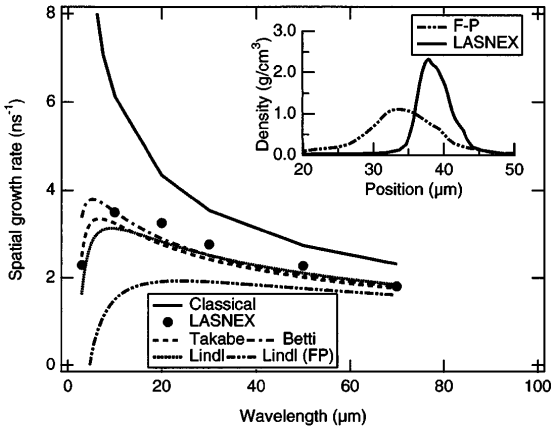

FIG. 6. LASNEX growth rates in spatial amplitude (γ_z) at the ablation surface. The predictions of Eqs. (2)–(4), the classical growth rates for this acceleration and the prediction of Eq. (3) for the conditions produced in a Fokker-Planck calculation are also shown. Inset: The density profiles at $t = 1.5$ ns for the LASNEX and FP calculations.

The discrepancy between the measured and predicted growth rates is slightly more than the experimental uncertainty (χ^2/ν of 2.2, or a confidence limit of about 10%). The average of the simulated growth rates is about 18% higher than the measured values. We considered several sources of systematic error in both the data and the modeling which may have an effect at this level. The acceleration is not measured on every shot, but the laser power is measured with an uncertainty of $\pm 15\%$; our simulations indicate that the uncertainty in growth rates due to this variation in laser power is about 5%. Another possible source of time-dependent error is the uranium backlighter spectrum; this was measured using absolutely calibrated time-resolved x-ray detectors (DANTE [24]) for the energy contribution less than 3 keV and a streaked spectrometer for the 3–4 keV contribution. While the magnitude of the emission increases with time, the shape of the spectrum varied only enough to change the contrast by about 3% between 1 and 3 ns. Thus the total experimental systematic error is estimated to be about $\pm 7\%$.

One possible source of systematic error in the simulations would be an incorrect prediction of the foil density as a function of time. Honda *et al.* [25] (HM) have calculated lower RT growth rates using 2D full Fokker-Planck (FP) simulations compared to Spitzer-Härm [26] (SH) electron transport, such as was used in the LASNEX simulations. The difference is due to a change in the longitudinal density profile resulting from preheat by energetic electrons originating in the plasma corona which penetrate beyond the ablation front. Such differences in 1D structure were noted earlier by Epperlein *et al.* [27]. We have simulated the foil acceleration in 1D using an approximation to the FP equation from Bhatnagar *et al.* [28] (BGK). We see similar changes to the density profile to those noted by HM; typical density profiles for BGK and SH are shown in the inset in Fig. 6. We have not simulated RT growth in 2D with FP or BGK transport, but we can estimate the effect upon the growth rate through the dispersion relation, Eq. (3). The predicted density scale length L is increased from 1 μm for SH to 3.5 μm, and the ablation velocity v_a from 1.1 to 1.3 μm/ns. The dispersion relation from Eq. (3), using these parameters, is also shown in Fig. 6. The growth rate is lower than that from the LASNEX simulations by an average of 20% for wavelengths between 20 and 70 μm. It is plausible that this electron transport effect could resolve the discrepancy between the measured growth rates and the LASNEX simulations. Increased experimental accuracy and experiments examining shorter modulation wavelengths are required to determine whether electron transport effects are indeed important for RT growth for direct drive ICF. HM present growth rates for a single wavelength $\lambda = 60$ μm, for which they obtain 1.4 ns^{-1} for FP vs 2.1 ns^{-1} for SH. The foil parameters considered by HM are nearly the same as those of this experiment. HM use Eq. (2) to fit their growth rates, so they must increase β to match the FP growth rate, whereas Eq. (3) predicts a growth rate reduction from the increase in L as well as that from the increase in v_a. Their growth rate for SH is close to the locus of LASNEX simulations, while the FP result is somewhat lower than the prediction of Eq. (3), using the BGK parameters.

In summary, we have determined Rayleigh-Taylor growth rates for modulations on planar foils accelerated by laser ablation. The growth rates varied between 1.5 and 2.1 ns^{-1} as a function of wavelength. The simulated growth rates were about 18% higher than the measured values with a 10% confidence limit. Systematic experimental errors do not appear large enough to resolve this discrepancy.

This work was performed under the auspices of the U.S. DOE by the Lawrence Livermore National Laboratory under Contract No. W-7405-ENG-48.

[1] J. Nuckolls *et al.*, Nature (London) **239**, 139 (1972).
[2] S. Bodner, Phys. Rev. Lett. **33**, 761 (1974).
[3] J. D. Lindl and W. C. Mead, Phys. Rev. Lett. **34**, 1273 (1975).
[4] C. Verdon, BAPS **38**, 2010 (1993).
[5] S. V. Weber, BAPS **40**, 1781 (1995).
[6] J. H. Gardner *et al.*, BAPS **39**, 1697 (1994).
[7] S. G. Glendinning *et al.*, Phys. Rev. Lett. **69**, 1201 (1992).
[8] M. Desselberger *et al.*, Phys. Rev. Lett. **65**, 2997 (1990).
[9] J. Grun *et al.*, Phys. Rev. Lett. **58**, 2672 (1987).
[10] A. J. Cole *et al.*, Nature (London) **299**, 329 (1982).
[11] S. N. Dixit *et al.*, Appl. Opt. **32**, 2543 (1993).
[12] S. Skupsky *et al.*, J. Appl. Phys. **66**, 3456 (1989).
[13] G. B. Zimmerman and W. L. Kruer, Comments Plasma Phys. Control. Fusion **2**, 51 (1975).
[14] O. L. Landen *et al.*, in *Ultrahigh- and High-Speed Photography, Videography, and Photonics '93*, SPIE Proceedings Vol. 2002 (SPIE–International Society for Optical Engineering, Bellingham, WA, 1993), p. 1.
[15] S. G. Glendinning *et al.*, in *Applications of Laser Plasma Radiation II*, SPIE Proceedings Vol. 2523 (SPIE–International Society for Optical Engineering, Bellingham, WA, 1995), p. 29.
[16] H. C. Andrews and B. R. Hunt, *Digital Image Restoration* (Prentice-Hall Inc., Englewood Cliffs, NJ, 1977).
[17] B. A. Remington *et al.*, Phys. Plasmas **2**, 241 (1995).
[18] S. Hann, Phys. Rev. A **39**, 5812 (1989).
[19] T. Endo *et al.*, Phys. Rev. Lett. **74**, 3608 (1995).
[20] S. Bodner, Phys. Rev. Lett. **33**, 761 (1974).
[21] H. Takabe, L. Montierth, and R. L. Morse, Phys. Fluids **26**, 2299 (1983); H. Takabe *et al.*, ibid. **28**, 3676 (1985).
[22] J. Lindl, Phys. Plasmas **2**, 3933 (1995).
[23] R. Betti *et al.*, Phys. Plasmas **3**, 2122 (1996).
[24] H. N. Kornblum, R. L. Kauffman, and J. A. Smith, Rev. Sci. Instrum. **57**, 2179 (1986).
[25] M. Honda and K. Mima, Phys. Rev. Lett. (to be published); also K. Shigemori *et al.*, Phys. Rev. Lett. **78**, 250 (1997).
[26] L. Spitzer and R. Härm, Phys. Rev. **89**, 977 (1953).
[27] E. M. Epperlein and R. W. Short, Phys. Fluids B **3**, 3092 (1991).
[28] P. L. Bhatnagar, E. P. Gross, and M. Krook, Phys. Rev. **94**, 511 (1954); W. E. Alley (private communication).